Characterizing Dissolved Organic Matter and Water-Soluble Compounds in Ground Ice of the Russian Arctic: A Focus on Sample Classification within the Carbon Cycle Context

Petr Semenov *, Anfisa Pismeniuk, Anna Kil, Elizaveta Shatrova, Natalia Belova, Petr Gromov, Sergei Malyshev, Wei He, Anastasiia Lodochnikova, Ilya Tarasevich, Irina Streletskaya, Marina Leibman

Posted Date: 14 December 2023

doi: 10.20944/preprints202312.1097.v1

Keywords: ground ice, dissolved organic matter, excitation-emission matrix fluorimetry, biogeochemical cycling, greenhouse gas emission

Article

Characterizing Dissolved Organic Matter and Water-Soluble Compounds in Ground Ice of the Russian Arctic: A Focus on Sample Classification within the Carbon Cycle Context

Petr Semenov [1,*], Anfisa Pismeniuk [2], Anna Kil [1], Elizaveta Shatrova [1,3], Natalia Belova [2], Petr Gromov [4], Sergei Malyshev [1], Wei He [5], Anastasiia Lodochnikova [1], Ilya Tarasevich [2,6], Irina Streletskaya [2] and Marina Leibman [6,7]

[1] All-Russia Institute of Geology and Mineral Resources of the World Ocean (VNIIOkeangeologia), 190121, Saint-Petersburg, Russia; p.semenov@vniio.ru (P.S.); a.kil@vniio.ru (A.K.); e.shatrova@vniio.ru (E.Sh.); s.malyshev@vniio.ru (S.M.); a.lodochnikova@vniio.ru (A.L.)

[2] Department of Cryolitology and Glaciology, Faculty of Geography, Lomonosov Moscow State University, 119991, Moscow, Russia; apismeniuk@geogr.msu.ru (A.P.); belova@geogr.msu.ru (N.B.); irinastrelets@geogr.msu.ru (I.S.)

[3] Department of Geochemistry, Institute of Earth Science, Saint Petersburg State University, 199034, St. Petersburg, Russia; st040722@student.spbu.ru (E.Sh.)

[4] A.P. Karpinsky Russian Geological Research Institute, 199106, St. Petersburg, Russia; petr_gromov@vsegei.ru (P.G.)

[5] School of Water Resources and Environment, China University of Geoscience Beijing, Beijing, 100083, China; wei.he@cugb.edu.cn (W.H.)

[6] Tyumen Scientific Centre SB RAS, Earth Cryosphere Institute, 625026, Tyumen, Russia; tarasevich.ilya1@gmail.com (I.T.); m.o.lejbman@utmn.ru (M.L.)

[7] Laboratory of Polar and Sub-Polar Geosystems, Institute X-BIO, University of Tyumen, 625003, Tyumen, Russia; m.o.lejbman@utmn.ru (M.L.)

* Correspondence: p.semenov@vniio.ru

Abstract: Climate-induced changes contribute to the thawing of ice-rich permafrost in the Arctic, which leads to the release of large volumes of organic carbon into the atmosphere in the form of greenhouse gases, mainly carbon dioxide and methane. Ground ice constitutes a considerable volume of the cryogenically sequestered labile dissolved organic carbon (DOC) subjected to fast mineralization upon thawing. In this work we collected an unique geochemical database of the ground and glacier ice comprising the samples from various geographic locations characterized by a variety of key parameters, including ion composition, carbon-bearing gases (methane and carbon dioxide) bulk biogeochemical indicators and fluorescent dissolved organic matter (DOM) fractions. Our results show that interaction with solid material—such as sediments, detritus, and vegetation—is likely the overriding process in enrichment of the ground ice in all the dissolved compounds. Terrigenous humic-like dissolved organic matter was predominant in all the analyzed ice samples except for glacier ice and pure tabular ground ice from Mare Sale (Western Yamal). The labile protein-like DOM, indicating an autochthonous source, showed no correlation to humic components and probably associated with microbial abundance in the ground ice. The sum of the fluorescent DOM components satisfactory correlates to DOC, indicating the adequacy of the estimation. The pure tabular ground ice samples exhibit the highest biogeochemical quality which may be responsible for the amplification of permafrost organic matter decomposition upon thawing. Yamal impure tabular ground ice and ice wedges are extremely enriched in methane compared to the samples from other locations which should cause a portion of direct methane emission upon the putative thawing.

Keywords: ground ice; dissolved organic matter; excitation-emission matrix fluorimetry; biogeochemical cycling; greenhouse gas emission

 doi:10.20944/preprints202312.1097.v1

1. Introduction

Climate-induced changes contribute to the thawing of ice-rich permafrost in the Arctic, which leads to the release of large volumes of organic carbon into the atmosphere and oceans. The mobilization of extra carbon in the modern biogeochemical cycle leads to an excess of greenhouse gases in the atmosphere, contributing to positive feedback [1]. Ice-rich permafrost, predominantly located in Russia, Canada, and Alaska, is distinguished by widespread ground ice: constitutional ice, ice wedges, and tabular ground ice. Thawing of ground ice in response to contemporary climate conditions leads to the active layer deepening, thermokarst, thermo-erosion, and slope processes, along with the release of carbon into the surrounding permafrost environments. The ground ice-bond carbon reservoir includes pre-formed carbon-bearing greenhouse gases (GHGs, mainly CH4 and CO2) and pre-aged organic matter (OM), represented by dissolved (dissolved organic matter, DOM) and particulate (particulate organic matter, POM) forms. The tabular ground in West Siberia has been reported to contain an enormously high amount of trapped microbial methane, which is responsible for the direct GHG emission upon the thawing of ground ice [2–4]. Although recent simulations have estimated the GHG emissions from the Yedoma deposits as only about 1% of the total permafrost GHG emissions [5], the impact of ground ice thawing on the carbon cycle is undoubtedly critical for both the local and regional ecosystems of the Arctic.

The ancient permafrost-derived organic matter has been reported for a relative enrichment in biochemically labile fraction. It is assumed that the rapid biochemical immobilization of the source OM as a result of the freezing contributed to a lower degree of the immobilized OM mineralization and, consequently, to a higher biochemical quality of the resulting permafrost-bound organic carbon reservoir [6]. The ground ice itself indicates the particular importance of dissolved organic carbon (DOC) as a storage form for trapped carbon. It has been reported that the Yedoma ice wedges store significant pools of DOC (45.2 Tg) and dissolved inorganic carbon (DIC) (33.6 Tg) [7]. Although DOM is involved in close interaction with POM, the most labile compounds, which are immediately available for microbial consumption, are dissolved in water. The ground ice DOC vulnerability to a modern transformation, finalized as GHG emissions, is obviously determined by the DOM composition, suggesting that more biolabile constituent is readily mineralized, but refractory/recalcitrant one is rather accumulated in the solution within the certain time scale, thus having a longer residence time. In the incubation experiments, the IW meltwater addition indicated the sizable increase of the DOC loss in Yedoma samples, suggesting that the low-molecular weight biolabile DOM of IW promoted the mineralization of predominantly high molecular weight recalcitrant Yedoma OM by co-metabolizing effect [8]. The excitation–emission matrix (EEM) fluorescence coupled with parallel factor analysis (PARAFAC) of the measured fluorophores is a conventional tool for investigating the molecular fractions of highly heterogeneous DOM composition in natural waters [9,10]. It allows extractions of the components of fluorescent DOM which can be assigned to whether allochthonous, recalcitrant/biorefractory, or autochthonous biolabile DOM fractions. The negative correlation between the DOC loss (biodegradable DOC, BDOC) and content of the most labile fraction of protein-like DOM has been detected as a result of the incubation tests, involving ground ice and permafrost samples [8,11]. The distribution of fluorescent DOM fractions might, to some extent, reflect the partitioning of the DOC pool into the portions with various vulnerability to microbial transformation, finally resulting in different amounts and ratios of the gaseous products: CO2 and CH4. This can be applicable to the modeling of GHG generation from permafrost soils and deposits, implying the indication of biochemical quality of the OM subject to mineralization upon thawing. Summarizing all the above, we may infer that the fluorescent DOM analysis is undoubtedly, very promising approach in studying the DOC and DOM biogeochemistry of the ground ice. Another application of the fluorescent DOM fractions data is paleoclimate reconstructions. This is based on the assumption that DOM composition reflects hydrological and climate conditions as well as local vegetation of the paleo environments. As it was shown in the previous work, the PARAFAC-DOM components distribution in the Faddevsky IWs (Kotelny Island, New Siberian archipelago) correlated with the age of the IW formation (Holocene

 doi:10.20944/preprints202312.1097.v1

and Late Pleistocene) and distinguished between the ice wedges and tabular ground ice within the sample collection [12].

In this study, we integrate data on water-soluble compounds in ground ice samples from various locations with significant geographic extents, including Kotelny Island (East Siberian Sea) and the Yamal Peninsula (Kara Sea). We address the following tasks in our work:

- To describe the variations of the available water-soluble compounds, including the carbon bearing gases (CH4 and CO2) within the dataset in terms of carbon cycling;
- To compose and validate PARAFAC model for the fluorescent DOM components in the database on ground ice from various locations in the Arctic;
- To trace the relationship between the dissolved organic carbon and the molecular fractions of DOM (PARAFAC components) and establish possible sources of the fluorescent DOM molecular fractions using available geochemical indicators;
- To estimate the water-dissolved/water-soluble geochemical parameters interrelation, sample variability and intrinsic diversity using a multivariate statistic (PCA).

2. Study area and dataset design

This article presents research conducted in the Russian Arctic, based on field data collected from five distinct key sites (Figure 1). The selection of these sites was driven by their geographical location, landscape features, and the type of ice. In total, we collected samples, comprising tabular ground ice (TGI) and ice wedges of various ages from Northwestern Russia, Western and Eastern Siberia. Furthermore, additional samples were taken from the Leningradsky glacier on Bolshevik Island in the Severnaya Zemlya archipelago to represent the reference for ground ice samples.

The westernmost site, located 5 km east of Amderma settlement on the Kara Sea coast, exposes the TGI in a retrogressive thaw slump (RTS) [13]. The stratified TGI is over 4.5 meters thick and is covered with loamy sediments containing fragments of mollusk shells. The stratification observed in the TGI arises from variations in the composition of soil and air inclusions within the ice. In the uppermost 1.5 meters of the TGI, the sediment content is notably high, including particles of silty, sandy, and pebble sizes. Pure ice layers tend to be rather thin, typically measuring less than 1 centimeter in thickness. The lower part of the TGI, located at depths ranging from 6 to 9 meters below the surface, represents interlayering of pure transparent ice, pure bubbly ice, and stratified ice. For this study samples (Table 1, AM.TGI/p 1 – 9) were collected from depths ranging between 6 and 7 meters beneath the surface.

Preprints (www.preprints.org) | NOT PEER-REVIEWED | Posted: 14 December 2023 doi:10.20944/preprints202312.1097.v1

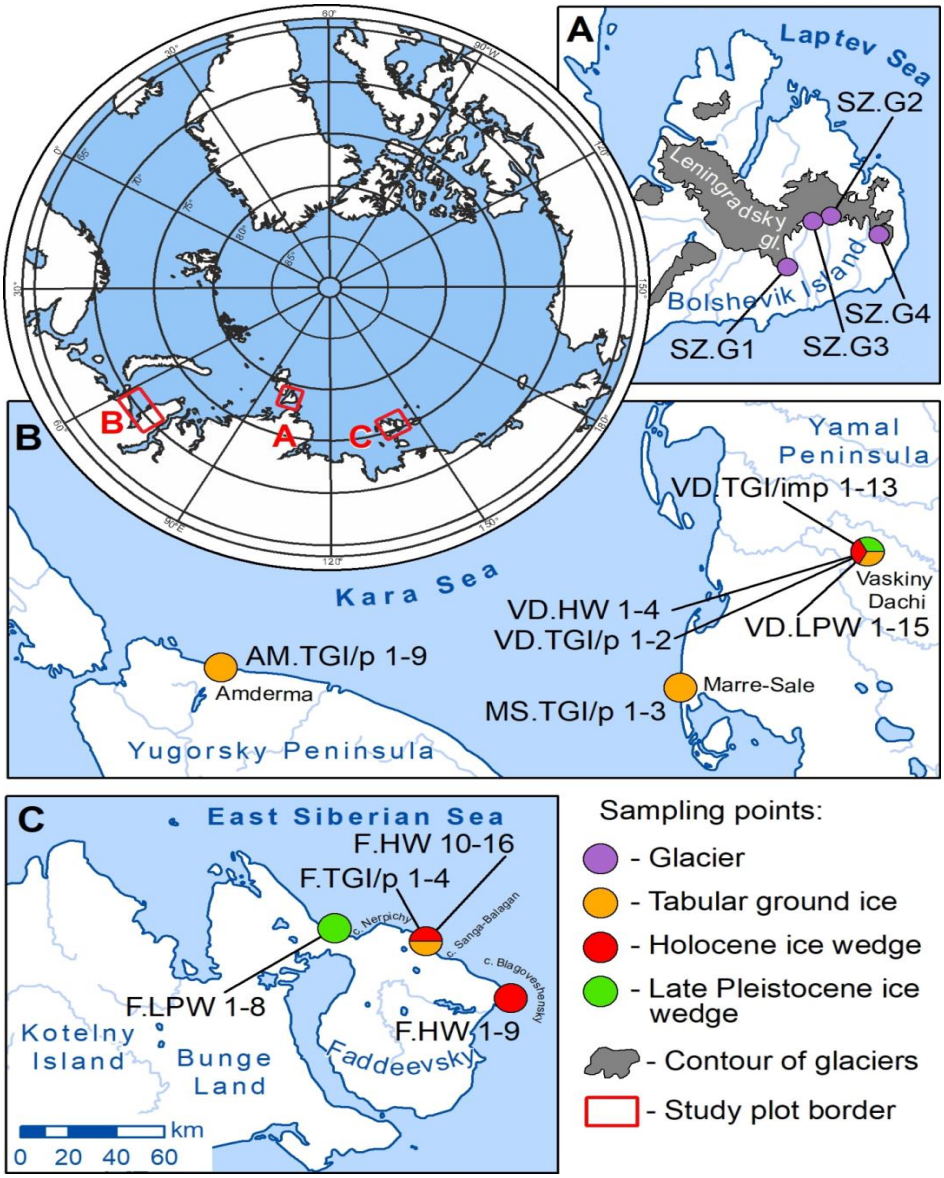

Figure 1. Study plots with sampling points. A - Bolshevik Island, Leningradsky glacier (4 samples - SZ.G 1-4). B - Yugorsky peninsula, Amderma (9 samples - AM.TGI/p 1-9); Yamal peninsula, Marre Sale (3 samples - MS.TGI/p 1-3), Vaskiny Dachi (34 samples - VD.TGI/imp 1-13, VD.HW 1-4, VD.TGI/p 1-2, VD.LPW 1-15). C - New Siberian Islands, Kotelny Island (28 samples - F.HW 10-16, F.TGI/p 1-4, F.LPW 1-8, F.HW 1-9).

In West Siberia, our research focused on the TGI and ice wedges at the Marre-Sale and Vaskiny Dachi research stations. At Marre-Sale, in 2022, we examined the TGI (TGI 1 type) [14] within a 25-meter-high coastal cliff along the Kara Sea (Figure 2 - B). The upper part of this cliff is composed of continental sandy deposits, which contain syngenetic ice wedges. The TGI is exposed at a depth of 11–12 m from the surface and consists of two adjacent lenses, measuring 0.4 and 0.75 m in thickness. The TGI samples (Table 1, MS.TGI/p 1 – 3) we collected do not contain any ground inclusions, and the ice is coarse-crystalline (Figure 2 - C), with individual crystals exceeding 10 cm in size, indicating a relatively slow freezing process.

Preprints (www.preprints.org) | NOT PEER-REVIEWED | Posted: 14 December 2023 doi:10.20944/preprints202312.1097.v1

Figure 2. Typical examples of ground ice exposures and samples. A – tabular ground ice (TGI) and ice wedge (IW) in RTS in Central Yamal (Vaskiny Dachi); B – TGI in the coastal outcrop (Marre-Sale, Yamal); C – pure TGI sample (Marre-Sale, Yamal); D – Glacier ice (Bolshevik, Severnaya Zemlya); E – the contact of the IW and impure TGI (Vaskiny Dachi, Yamal); F – TGI sample (Vaskiny Dachi, Yamal); G – Holocene IW (Faddeevsky, New Siberian Islands); H – Holocene IW sample (Faddeevsky, New Siberian Islands).

At the Vaskiny Dachi Research Station, located on the watershed of the Se-Yakha and Mordy-Yakha rivers in the central part of the Yamal Peninsula, we studied TGI and IWs found within a retrogressive thaw slump (RTS) headwall in 2021 (Figure 2 - A). The upper border of the TGI lies at a depth of 3.0 meters (at an absolute height of 22 m) beneath the surface and is covered by Late Pleistocene-Holocene continental deposits. The TGI is characterized by layers of transparent ice intermixed with dark sandy loam (Figure 2 - F). In the middle segment of the section, the pure ice layers measure over 5 cm thick (Table 1, VD.TGI/p 1 – 2). The TGI is interrupted by Late Pleistocene IW (Figure 2 - E) with a visible height of 3.5 m and a width of 0.7 m in the upper part. We collected samples from both the IW (Table 1, VD.LPW 1 – 15) and the TGI (Table 1, VD.TGI/imp 1—13) throughout the entire depth of the ice wedges. Additionally, we examined Holocene ice wedges from the Vaskiny Dachi Research Station, located within the polygonal peatland. The polygons can reach sizes of up to 10 m in diameter, surrounded by polygonal troughs 0.3 – 0.5 m wide. Within the polygonal troughs, starting from depths of 0.5-0.6 meters, we sampled the top of Holocene IW (Table 1, VD.HW 1 – 4). The wedge ice is transparent with characteristic sub-vertical layering and peat inclusions in lateral parts.

In the East-Siberian Arctic, we investigated ground ice on the Faddeevsky Peninsula, Kotelny Island, and the New Siberian Archipelago described in [12]. Briefly, we collected Yedoma IW samples (Table 1, F.LPW 1 – 8) near the Cape Nerpichy from the upper part of a 12-meter cliff. Close to Cape Sanga-Balagan and Blagoveshensky, we sampled Holocene ice wedges (Table 1, F.HW 1 – 16) found in coastal cliffs ranging from 3 to 6 m in height (Figure 2 – G; H). The Holocene continental complex of deposits containing ice wedges is underlain by marine clays formed before MIS 3. In proximity to Cape Sanga-Balagan, we also investigated transparent tabular ground ice (Table 1, F.TGI/p 1 – 5) with some mineral inclusions at the height of 9 m. The origin of the TGI remains unclear [12].

To compare our ground ice results with glacier ice, we collected four surface samples from the South-Eastern part of the Leningradsky glacier, located along its southern border on Bolshevik Island in the Severnaya Zemlya archipelago. Leningradsky is a complex glacier with an approximate area

 doi:10.20944/preprints202312.1097.v1

of 2300 km², comprising 4 ice caps, 11 outlet glaciers, and 3 slope glaciers [15]. The age of the glacier remains uncertain. Ice core dating for the Akademii Nauk glacier suggests an age of 2.5 ka BP [16], while another study by [17] proposes an age of 12 ka BP. The Vavilova glacier is reported to have an age of 8-9 ka BP [17]. The sampling site SZ.G1 is situated in the southernmost part of shield #56 (for further reference, glacier numbers are from [15; P.36-37]). The sample was obtained from the glacier's edge. Sample SZ.G2 was taken from ice cap #57, 270 meters inward from the glacier's border. Sample SZ.G3 was collected from outlet glacier #68, 700 meters inward from the glacier's border. Sample SZ.G4 was obtained from ice cap #59, which became separated from the complex Leningradsky glacier due to melting over the past 40 years. SZ.G4 is located in the vicinity of the glacier's highest point, approximately 2 km inward from its nearest border. All ice samples were transparent with a light-blue tint (Figure 2 - D), containing air bubbles, and were collected from depths of 10-15 cm.

While some of the sampling points have been previously documented by authors [12,13], this article introduces a new dataset and sampling structure based on the location and the type of ice. We have assigned different names to these sampling points and samples, thus, additional details regarding their former names can be found in Tables S1 and S2. Sample names have been designed to convey maximum information about each sample, including its location (e.g., SZ - Severnaya Zemlya, Bolshevik Island; AM - Yugorsky Peninsula, Amderma site; VD - Yamal, Vaskiny Dachi site; MS - Yamal, Marre-Sale site; F - New Siberian Islands, Faddevsky). The ice type is indicated by G for glacier ice, W for ice wedges, and TGI for tabular ground ice. In the case of TGI samples, the sediment content, which significantly influences DOM composition, is specified. Ice samples are classified as pure when the sediment content is less than 10% (by mass) of the solid fraction (TGI/p) and as impure when the sediment content exceeds 10% (TGI/imp). Additionally, ice wedge samples are further categorized by age into Late Pleistocene (LP) and Holocene (H). An overview of this new dataset structure is provided in Table 1.

Preprints (www.preprints.org) | NOT PEER-REVIEWED | Posted: 14 December 2023 doi:10.20944/preprints202312.1097.v1

Table 1. Sampling points and dataset design.

Region	Location	Type of Ice	Age of Ice Wedges	Solid fraction content	Group of samples
Yugorsky Peninsula	Amderma 69°44′53″N 61°47′17″E	TGI		pure	AM.TGI/p 1 — 9
Yamal Peninsula	Vaskiny dachi 70°16′03″N 68°55′22″E	TGI	Late-Pleistocene Holocene	pure	VD.TGI/p 1 — 2
		TGI		impure	VD.TGI/imp 1 — 13
		IW			VD.LPW 1 — 15
		IW			VD.HW 1 — 4
	Marre-Sale 69°42′14″N 66°48′30″E	TGI		pure	MS.TGI/p 1 — 3
New Siberian Islands	Faddeevsky, Kotelny Island 75°46′23″N 144°8′18″E	TGI		pure	F.TGI/p 1 — 5
	75°50′10″N 142°47′37″E	IW	Late-Pleistocene		F.LPW 1 — 8
	75°31′03″N 145°20′49″E	IW	Holocene		F.HW 1 — 16
Severnaya Zemlya	Leningradsky glacier, Bolshevik 78°24′42″N 103°17′54″E	Glacier			SZ.G1
	78°37′44″N 104°4′36″E				SZ.G2
	78°36′21″N 103°45′05″E				SZ.G3
	78°32′39″N 104°54′60″E				SZ.G4

For box-plots representation we split our dataset in 3 categories: impure TGI (TGI/imp, n=13), pure TGI (TGI/p, n=18) and IW (W, n=43) by combining the distinct groups of the ground ice samples.

3. Materials and Methods

During the study we processed 78 ice monoliths, including glacier and ground ice following the scheme described in the previous section. The methodology of the ice sample preparation was described in detail in our previous papers [12,18].

3.2. Solid fraction content.

The ica monoliths were weighted before further preparations. After thawing of the ice monoliths at +4 ^{0} C, the supernatant melt water was taken for filtration and dissolved compounds analysis, the precipitated solid part was freeze-dried and weighted. The weight of the coarse filter from supernatant was summed with the weight of the freeze-dried residue and related as % to the initial monolith weight.

 doi:10.20944/preprints202312.1097.v1

3.2. Ion composition

Ion composition of filtered thaw-water samples was analyzed using ion chromatography Metrohm 940 Professional IC Vario with a conductometry detector and a chemical suppressor unit (MSM-A). The anions were separated on Metrosepp A Supp 5–250/4.0 column, using 5 mmoL Na2CO3/NaHCO-3 solution as an eluent with flow rate 1 mL/min. The cations were separated on column Metrosepp C6–250/4.0 with a mixture of 1.7 mM nitric and 1.7 mM dipicolinic acid solution at a flow rate of 0.9 mL/min. The certified standard mixtures of ion composition (Fluka) were utilized to calculate the concentrations (mg/L). The uncertainty of the analytical measurements was ±1.5%. The detection limit was 0.02 mg/L (Cl-). The total dissolved ions content (TI) was determined as the sum of all ions, excluding dissolved carbonates represented as dissolved inorganic carbon (DIC).

3.3. Bulk biogeochemical parameters

Dissolved carbon species (DOC and DIC) were measured using the Shimadzu TOC-V element analyzer. The uncertainty of the analytical measurements was no higher than ± 6%. Detection limit was not exceeding 0.05 mgC/L. Dissolved inorganic nitrogen (DIN) was calculated as a sum of NO3− and NH4+ related to carbon content.

3.4. Gas Analysis

Gas chromatographic (GC) analysis of CH4 in the headspace of a thaw-water was made on a Shimadzu GC 2014 gas chromatograph equipped with Restek Rt-Aluminia BOND / Na2SO4 (40 m) wide bore capillary column and flame ionization detector (FID). Helium was utilized as a carrier with 25 ml/min flow rate. For CO2, concentration measurements we used a Porapak-N packed column (1m) and a thermal conductivity detector (TCD).

The certified gas mixtures were used for the method calibration. The uncertainty of the GC measurements was no higher than ± 5%. The detection limits were ~0.1 ppmV for CH4 and ~1 ppm for CO2, respectively. Methane concentrations (ppmV) were calculated using the values of headspace mixing ratio and Bunsen solubility coefficients [19]. It must be noted that the CO2 concentration in headspace gas of the meltwater samples presented in this work cannot be reliably compared to the CO2 concentrations measured as result of dry ice extraction, ultimately releasing the bubble gas composition, but not including the dissolved fraction [20,21].

3.5. Fluorescence Measurements of Dissolved Organic Matter Molecular Composition

Shimadzu RF5301 PC fluorimeter was applied for fluorescent excitation–emission matrix (EEM) measurements with wavelength ranges of 250–370 nm for excitation and 300-500 nm for emission of fluorescence. The fluorophores of the EEM matrix spectra were deconvoluted by PARAFAC modeling using the Matlab GUI (graphic user interfaces) toolbox efc v1.2 (https://www.nomresearch.cn/efc/indexEN.html) [22,23] and fluorescent DOM correction [23]. A dataset comprising 256 3D EEM spectra, including ice thaw water samples, along with the natural water samples from adjacent areas (stream, lake water) employed for PARAFAC modeling. The resulting PARAFAC model was tested through the sum of squared errors estimation (SSE), core consistency and split-half validation procedure [24]. The relative concentration of each PARAFAC component in Raman units (RU) was acquired as Fmax output of random initialization analysis [10]. The modified Tucker's Congruence coefficient values (mTCC) were employed to compare the identified PARAFAC components with library data containing 38 PARAFAC models [25].

3.6. Statistics

Descriptive statistics represented in this work included minimum, maximum, medium values, standard deviation and coefficient of variation calculated for each of the 9 ground ice samples groups (Tables S1 and S2). We used non-parametric Kruskall-Wallis multiple test for comparison of ground ice samples groups to estimate the reliability of variations (at $p < 0.05$). Prior to Principal components analysis (PCA) all the values in the dataset were Box-Cox transformed, the initial and resulting data

Preprints (www.preprints.org) | NOT PEER-REVIEWED | Posted: 14 December 2023 doi:10.20944/preprints202312.1097.v1

points distributions were analyzed with the Shapiro-Wilks test. The PCA was performed using 16 variables and 78 samples. The eigenvectors of the variables and the factor scores of the data were represented as biplot. All the statistical analyses were conducted using StatSoft STATISTICA 12.

4. Results

4.1. Solid fraction content and ion composition of the ground ice

The solid fraction content (S%) exhibits significant variability within our ground ice dataset as approved by the coefficient of variation (CV) of 189.0%. The highest S value (68.65%) indicating the extremely high solid fraction content in the ground ice sample is detected in the impure TGI (VD.TGI/imp 9) sampled from the ground ice exposure of the Vas'kiny Dachi site (Central Yamal). The lowest S values, suggesting insignificant solid matter inclusions in the ice body (<0.01 %), are characteristic of pure TGI from Marre sale site (Western Yamal). On the box plot (Figure 3) there is an obvious separation of the impure TGI in which the ice content is minor relative to the solid one (S%), represented either by soil or sediment particles in the thawed ground ice monoliths. The statically confident difference in solid fraction percentage is demonstrated between each of the three sample categories (TGI/p, TGI/imp, W) by the Kruskall-Wallis multiple test, with p value of 0.048 for the pair TGI/p and W, and $p < 0.0000$ for the pairs TGI/imp, TGI/p and TGI/imp, W respectively. The sequence of the sample categories with decreasing median values of solid fraction content (S, %) is TGI/imp (39.96%) > W (1.6%) > TGI/p (0.6%). The sequence of individual sample groups with decreasing S (%): VD.TGI/imp (39.96%) > VD.LPW (3.74%)> VD.TGI/p (1.81%) > F.HW (1.15%) > AM.TGI/p (0.86%) > F.LPW (0.35 ppmV) > F.TGI/p (0.14%) > MS.TGI/p (0.01%).

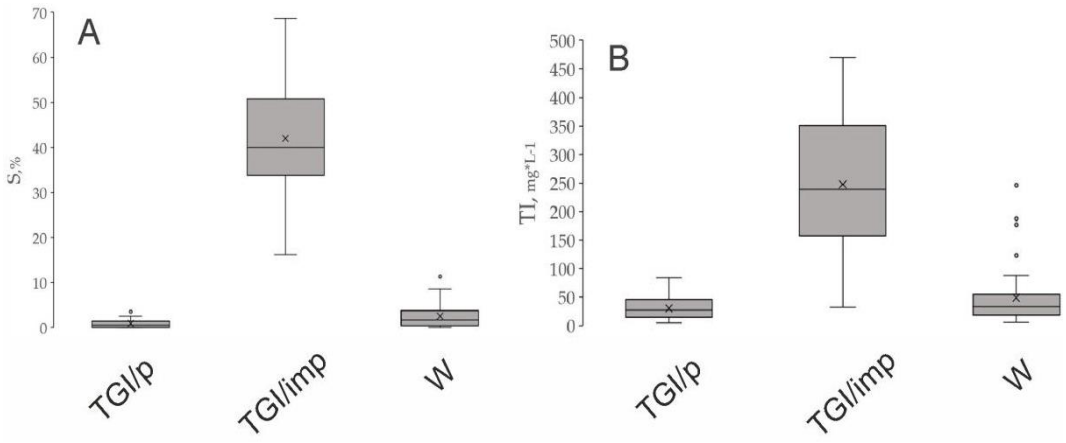

Figure 3. Box-plot of the solid fraction content, S (A) and total ion content TI (B) in the ground ice samples categories (TGI/p, TGI/imp and W).

The median ions concentrations as well as basic descriptive statistics for each group of the samples are given in the Tables S1 and S2. The most abundant ions in our ground ice sample collection (n=78) are Na+ and Cl-, respectively constituting 31.85 and 42.90 % of a sum of the ions (excluding HCO3- and CO32-) marked as Total ion, TI (mg/L). The sequence of decreasing median values of the ion percentage for a whole dataset is: Cl-(42.90%) > Na+(31.85%) > SO42-(8.06%) > Ca2+(4.50%) > K+(3.48%) > Mg2+(3.30%) > NH4+(1.30%) > NO32-(0.34%) > PO43-(0.12%). In this work we use the individual ions concentrations along with their sum (TI, mg/L) in multivariate statistics analysis for better separation of the sample groups on a PCA biplot as described in the Section. Thus, we do not address the particular distribution of each ion in our dataset. The ions abundance (TI, mg/L) is of great variation samples, indicated by CV=132.08%. The distribution of TI in the categories of ground ice is illustrated by box plot (Figure 4). The statistically reliable variance (p=0.0000) is marked for TGI/imp with both TGI/p and IW.

Preprints (www.preprints.org) | NOT PEER-REVIEWED | Posted: 14 December 2023 doi:10.20944/preprints202312.1097.v1

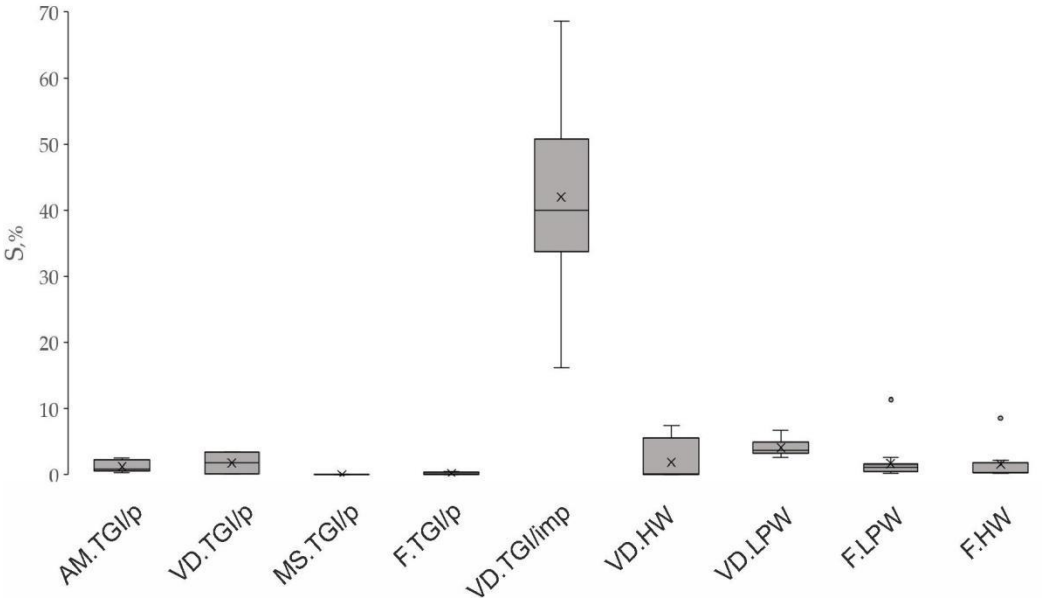

Figure 4. Box-plot of the solid fraction content (S,%) in the groups of the ground ice samples.

4.2. Bulk dissolved biogeochemical parameters (DOC, DIC, DIN) concentrations and distribution

Data on bulk biogeochemical parameters concentrations (DOC, DIC, DIN), including the descriptive statistics, are listed in the Tables S1 and S2. Regarding DOC content, the sample categories make up a sequence of decreasing values: TGI/imp>W>TGI/p (Figure 5) with a reliable inercategory variability approved by the non-parametric Kruskall-Wallis multiple comparison test at $p<0.0002$. The median DOC level (66.65 mg/L) in the impure TGI samples from Vaskiny Dachi site (VD.TGI/imp) is about 33 times higher than those of the pure TGI (TGI/p) combined group. The detected maximum of DOC concentration is as high as 111.00 mg/L in the impure TGI sample (VD.TGI/imp 11), while minimum one is as low as 0.85 mg/L in the pure TGI from Amderma site (AM.TGI/p 2). Variation of DOC level between the individual groups of samples naturally reveals that impure TGI samples from Yamal are sufficiently enriched in DOC relative to other groups (Figure 6). The sequence of decreasing DOC median values in the groups of the samples is VD.TGI/imp (66.65 mg/L) > F.LPW (13.01 mg/L) > VD.LPW (10.71 mg/L) > VD.HW (9.81 mg/L) > F.HW (7.60 mg/L) > F.TGI/p (4.4 mg/L) > VD.TGI/p (3.35 mg/L) > AM.TGI/p (1.74 mg/L) > MS.TGI/p (1.51 mg/L) > SZ.G (1.38 mg/L). To illustrate the variation of DOC in the sample groups, the anomalous VD.TGI/imp were excluded from the box-plot on Figure 6 - B. The Holocene IWs from Vaskiny Dachi are notable for the extreme outlier (VD.HW 3) with DOC value (84.39 mg/L), whereas other VD.HW samples have DOC content below 10 mg/L.

Maximum DIC concentration (35.50 mg/L) is also detected in the impure TGI sample (VD.TGI/imp 11), the minimum – in the pure TGI from Vaskiny Dachi site (VD.TGI/p 2). The median values in TGI/imp, TGI/p and W sample categories constitute 16.73, 3.97 and 2.82 mg/L respectively. The variance between TGI/imp and other sample categories (TGI/p and W) is statistically significant at $p<0.0002$. Maximum DIN level (3.47 mg/L) is observed in the Holocene IW from Vaskiny Dachi site (VD.HW 3), the minimum of 0.029 mg/L, close to the instrumental detection limit, is recorded in the pure TGI from Amderma site (AM.TGI/p 9). The median DIN values in TGI/imp, TGI/p and W sample categories constitute 0.73, 0.18 and 0.36 mg/L respectively. The increased level of DIN in TGI/imp samples is statistically significant, relative to both TGI/p and W ($p<0.05$).

Preprints (www.preprints.org) | NOT PEER-REVIEWED | Posted: 14 December 2023 doi:10.20944/preprints202312.1097.v1

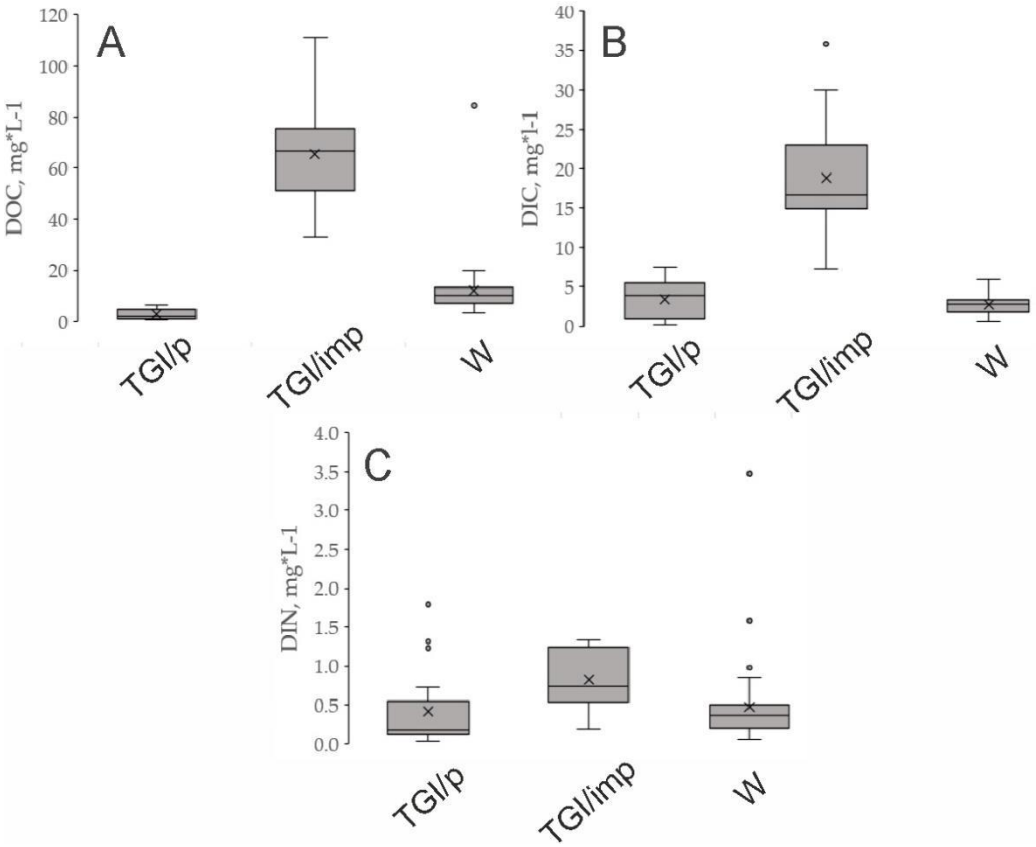

Figure 5. Box-plots of bulk biogeochemical parameters distribution: DOC (A) , DIC (B) , DIN (C) in the ground sample categories.

Preprints (www.preprints.org) | NOT PEER-REVIEWED | Posted: 14 December 2023 doi:10.20944/preprints202312.1097.v1

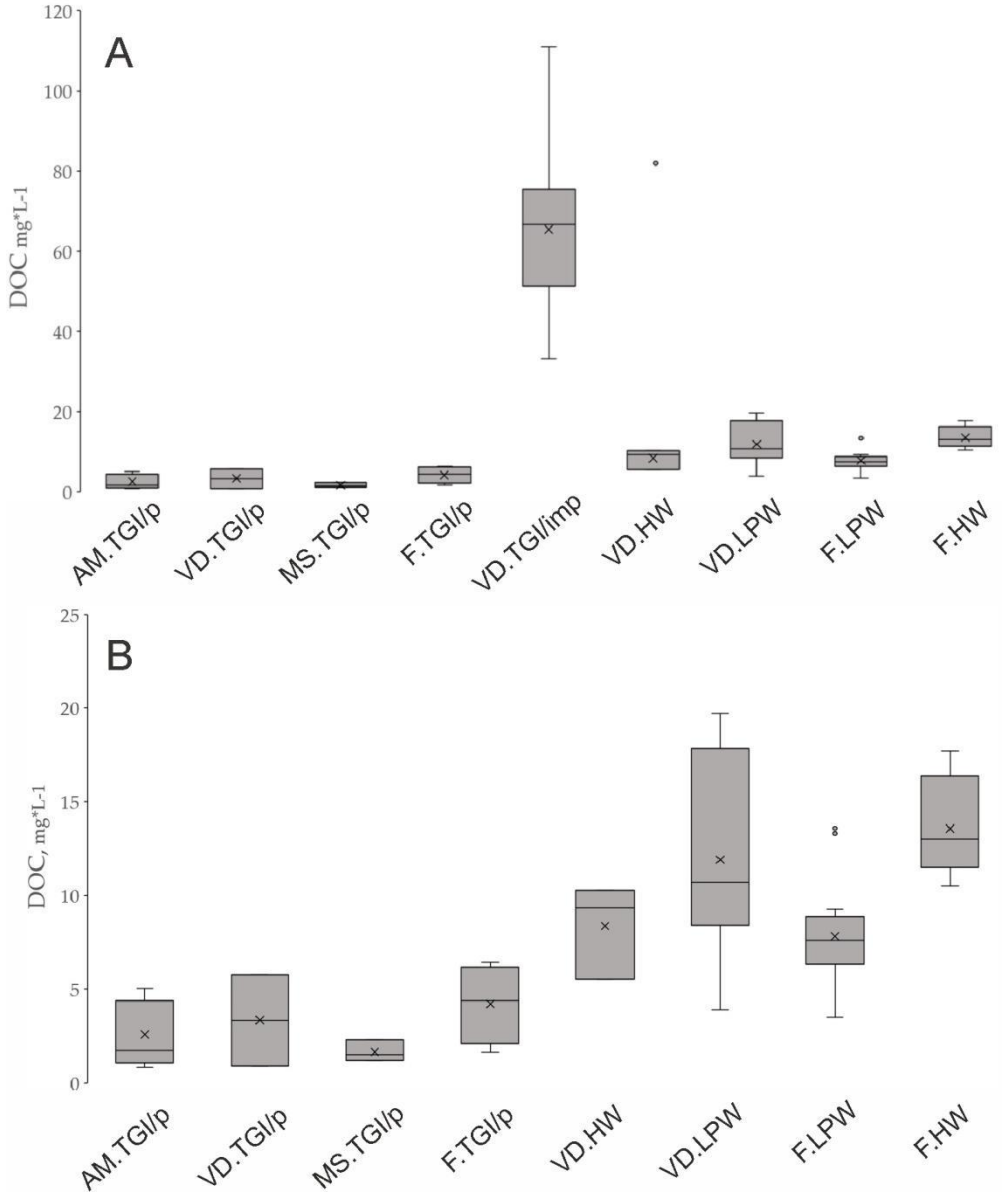

Figure 6. Box - plots of DOC distribution in the individual groups of the ground ice samples: A - all the groups of ground ice samples, B - the groups of the samples, excluding the anomalous values (VD.TGI/imp).

4.3. Carbon-bearing gases (CH4 and CO2) concentrations and distribution

Methane (CH4) concentration variations are highest among the analyzed geochemical variables as indicated by the coefficient of variation (CV) as high as 244%. The maximum CH4 concentration (32281.65 ppmV) is detected in the impure TGI from Yamal (VD.TGI/imp 13) and the lowest (0.391 ppmV) in the Late Pleistocene IW from Faddeevsky (F.LPW 6). The median methane concentrations in the ground ice samples categories make up a row: TGI/imp (5075.57 ppmV) > W (3009.ppmV) > TGI/p (5.14 ppmV). The corresponding box-plot diagram is represented on Figure 7. The Kruskall-Wallis multiple test reveals a significant variance between the TGI/imp and other categories (TGI/p and W) at level of $p<0.001$. However, a comparison between the individual groups of the ground ice samples shows that Late Pleistocene IWs from Yamal are reliably enriched in CH4, compared to the other groups ($p<0.001$) with the single outlier. The Holocene IW from Yamal (Vaskiny Dach site) are remarkable for a single outlier value (418.14 ppm) in the sample VD.HW 3, while other samples of this group express the CH4 concentration below 10 ppmV. The sequence of decreasing median values of methane content in the individual group is: VD.TGI/imp (5075.57 ppmV) > VD.LPW (3009.33

Preprints (www.preprints.org) | NOT PEER-REVIEWED | Posted: 14 December 2023 doi:10.20944/preprints202312.1097.v1

ppmV) > F.TGI/p (983.66 ppmV) > VD.TGI/p (23.72 ppmV) > VD.HW (8.66 ppmV) > F.HW (5.46 ppmV) > AM.TGI/p (4.55 ppmV) > F.TGI/p (1.79 ppmV) > F.LPW (1.29 ppmV).

The carbon dioxide (CO2) concentrations vary from 43.120 ppmV (a minimum value) in the pure TGI of the Amderma site (AM.TGI/p 8) to a maximum of 3539 ppmV in the Holocene IW of the Vaskiny Dachi site (VD.HW 3). The median CO2 concentrations in the ground ice samples categories indicate the row: TGI/imp (786.35 ppmV) > W (403.74 ppmV) > TGI/p (59.19 ppmV). The box-plots of CH4 variation in the individual groups are shown on Figure 8. To illustrate the variation of DOC in the sample groups, the anomalous VD.TGI/imp were excluded from the box-plot on Figure 8 - B.

The box plots of the CH4 and CO2 median concentrations variations in the categories of samples are shown on Figure 7.

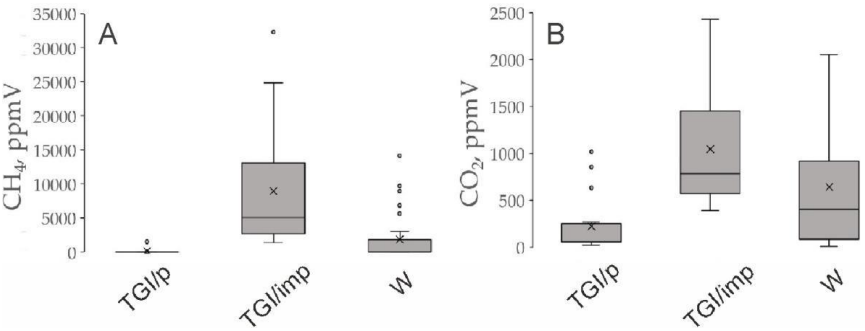

Figure 7. Distribution of carbon-bearing gases: CH4 (A) and CO2 (B) in the categories of the ground ice samples.

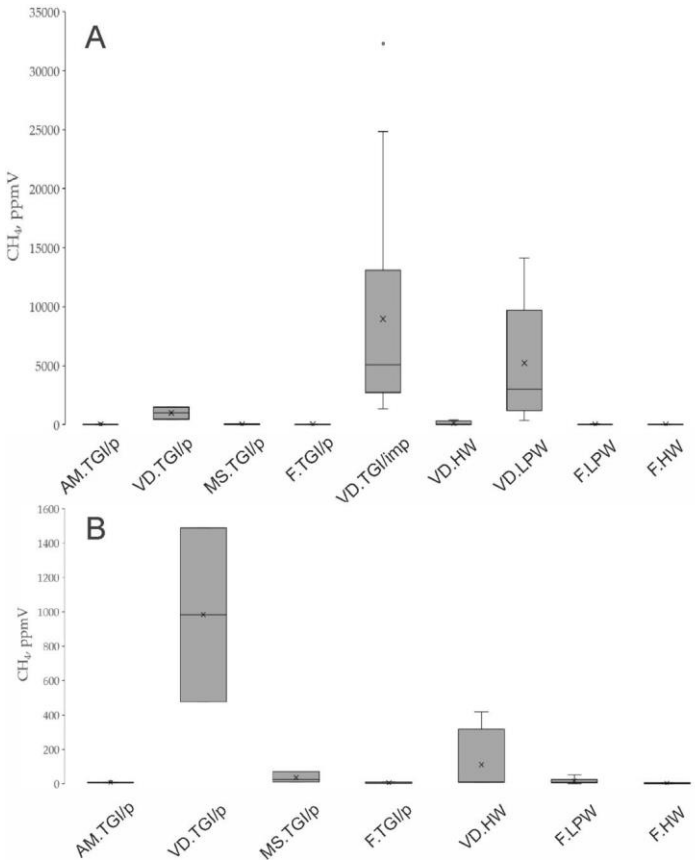

Figure 8. Distribution of methane (CH4) in the groups of the ground ice samples. A - all the groups of ground ice samples, B - the groups of the samples, excluding the anomalous values (VD.TGI/imp, VD.LPW).

 doi:10.20944/preprints202312.1097.v1

4.4. Fluorescent dissolved organic matter composition and distribution

The employed EEM dataset is composed of 252 samples, including the ground ice (TGI, IW), glacier ice and other natural water samples from adjacent areas (thaw water streams and thermokarst lakes), which are not included in our dataset of geochemical variables. Four fluorescence components were extracted from EEM spectra and validated for the dataset by PARAFAC analysis. Three components (P1, P2, P3) were recognized as humic-like DOM, and one is protein-like (tryptophan-like DOM). In Table 2 the spectral characteristics of the extracted fluorophores are indicated as well as the results of the library search using the EFC software. The representative EEM matrices illustrating the typical EEM fingerprints of the different ground ice types are exhibited on Figure 9. Among the obtained components, the humic ones (P1, P2, P3, P4) quite well correlate to each other (as indicated by the Pearson's correlation values indicated in the Table 2), but the protein-like component (P4) was equally not related to any of the other fractions.

The relative abundances of the EEM PARAFAC compounds (%) based on their median concentrations (RU) clearly indicate the character of the fluorescent DOM composition intergroup variability (Figure 10). Thus, the protein-like component P4 is making up >88% of the net DOM in the samples of Leningradsky glacier, Bolshevik island (SZ.G) DOM; > 81% of the pure TGI DOM from Marre-Sale (MS.TGI/p); > 46% of the pure TGI from the Fadeevsky Peninsula (New Siberian Island, F.TGI/p); > 15% of the pure TGI from the Yugorsky peninsula (Amderma site, AM.TGI/p). In the other groups of the analyzed ground ice samples, the contribution of P4 varies from 11.53 % in the Holocene IWs of Faddeevsky (F.HW) to the minimum value of 1.1% in the Holocene IW from the Vaskiny Dachi site. Among the humic-like DOM, the component P1 is the most ubiquitous in the majority of the sample groups, excluding the SZ.G, and MS.TGI/p, reported for outstanding abundance of P4. The maximum rate of P1 (83.2%) is characteristic of the impure TGI from Central Yamal (VD.TGI/imp). The P2 DOM is the minor humic-like species with contribution ranging from 1.73% in the samples of Leningradsky glacier, Bolshevik Island to 6.03% in the pure TGI of Marre Sale site (MS.TGI/p). The component P3 is a second number in abundance after P1 and the first number for a fluorescent DOM composition in the scope of a variation (CV=167.4%), reaching its maximum (33%) in the Late Pleistocene IW of Faddeevsky (Kotelny, New Siberian Islands), while drops to 0.3% in SZ.G.

A linear regression between the fluorescent DOM content (as sum of the P1-P4) and DOC concentration indicates a good fit between these parameters (r^2=0.96, p=0.0000). On the plot (Figure 11) we observe a clear separation of the samples extremely enriched in both DOC and fluorescent DOM, including all the impure TGI (VD.TGI/imp) and one Holocene IW sample (VD.HW). Other samples form a cloud of data points with visible scattering around the regression line. When examined separately the samples with DOC concentrations below 30 mg/L show the lower correlation between DOC and fluorescent DOM (r^2=0.54, p=0.0000) (Figure 11).

Concerning the P1 component each of the categories reveals the statistically significant variation ($p<0.005$) from any other as approved by the Kruskall-Wallis ANOVA test. The sequence of the decreasing P1 contents is impure TGI (TGI/imp) > Ice wedges (IW) > pure TGI (TGI/p).

The P2 component is highly variable in the TGI/p and quite homogenous in the TGI/imp samples. There is a significant difference ($p<0.005$) between TGI/imp and both TGI/p and IW. TGI/p and IW are not statistically distinct, however TGI/p shows higher average value than IW. The component P3 indicates the sequence of decreasing values: TGI/p > IW > TGI/imp, identical to the defined d for P2. The TGI/p samples appear to be especially enriched in protein-like DOM, represented by the P4 component. The observed order of decreasing values of P4 is TGI/p > IW > TGI/imp with all the inercategory differences statistically approved by Kruskall-Wallis ANOVA. The box plots of the CH_4 and CO_2 median concentrations variations in the categories of samples are shown on Figure 7. The box-plots of the EEM PARAFAC components variation in the categories of the ground ice samples are shown on Figure 12.

Preprints (www.preprints.org) | NOT PEER-REVIEWED | Posted: 14 December 2023 doi:10.20944/preprints202312.1097.v1

Table 2. Spectral characteristic of the extracted PARAFAC compounds including results of the comparison with previous studies through EEM library search (EFC software). The mTCC is a modified Tucker's congruence coefficient values [10,23].

Component	Emission maxima	Excitation, max	Description	Comparison with previous study (library search)
P1	470	370	Humic like	mTCC=0.97; humic-like,but not quinone-like [26]
P2	425	310	Humic like	mTCC=0.99, terrestrial or ubiquitous humic-like components, a photoproduct or a photorefractory component [27]
P3	470	260	Humic like	mTCC =0.97, humic-like, UV and visible, terrestrial, a bio-refractory component [28]
P4	340	270	Protein-like	mTCC=0.90. tryptophan-like, more biodegradable [27]

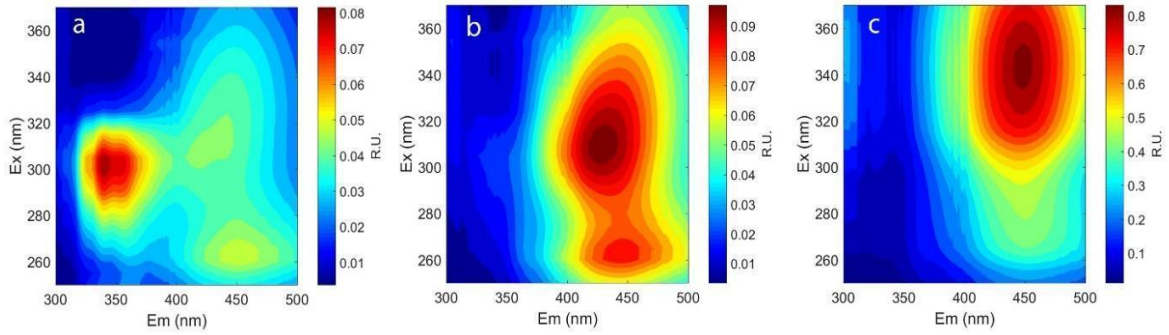

Figure 9. Representative EEM PARAFAC fluorograms of the various samples (pure TGI, obtained through random initialization of the 4 components PARAFAC model. a - pure TGI (AM.TGI/p 7); b - Late Pleistocene IW (VD.LPW); c - impure TGI (VD.TGI/imp).

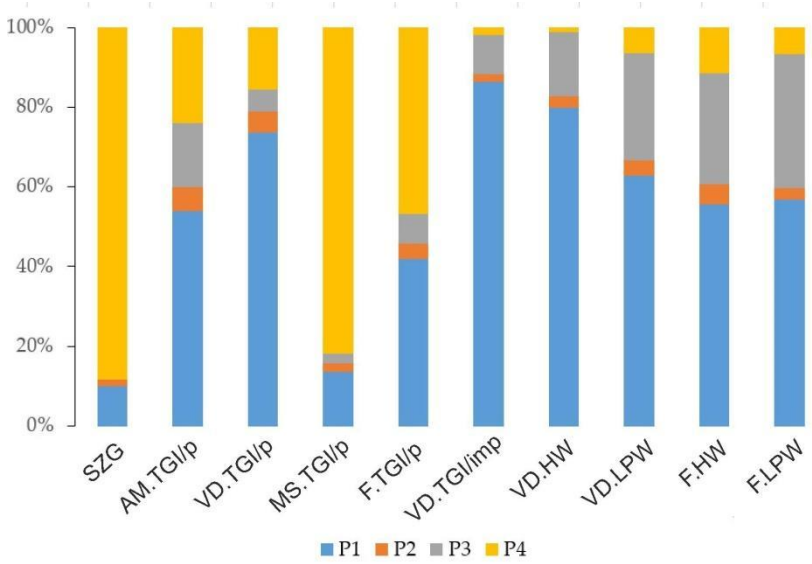

Figure 10. Relative abundance of the EEM PARAFAC compounds in various groups of the ice samples.

Preprints (www.preprints.org) | NOT PEER-REVIEWED | Posted: 14 December 2023 doi:10.20944/preprints202312.1097.v1

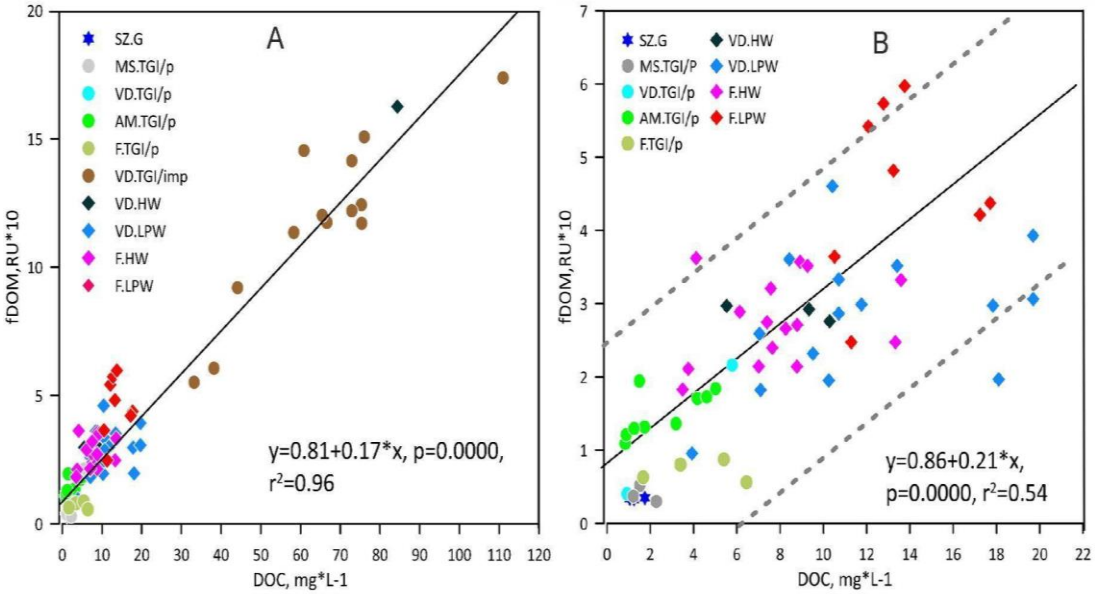

Figure 11. Linear regression of the fluorescent DOM (fDOM) content (as sum of all PARAFAC components) and DOC concentration. A - all the groups of ground ice samples, B - the groups of the samples, excluding the anomalous VD.TGI/imp.

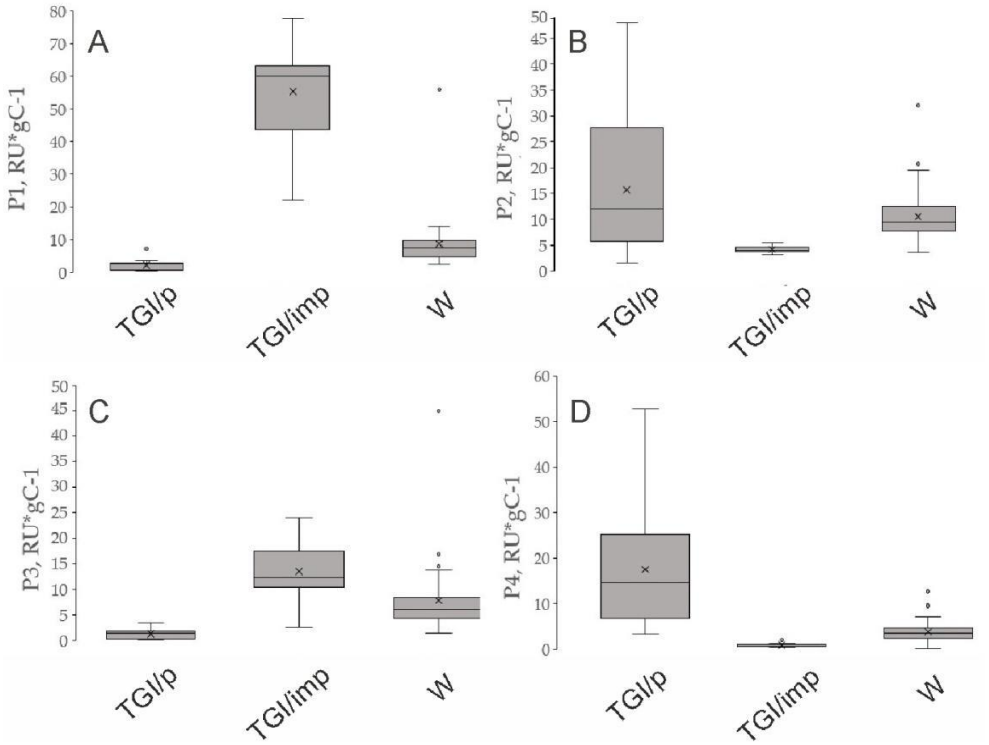

Figure 12. Box-plots of DOC-normalized values of the EEM-PARAFAC components, P1 (A), P2 (B), P3 (C), P4 (D).

4.5. Results of principal component analysis: the variables interrelation and data classification

The first 2 principal components explained the 83.61% of the total variance in the dataset with 50.26% and 15.06% covered by PC1 and PC2 correspondingly. It can be seen from the PCA biplot on Figure 13, that all the variables positively correlate to each other as detected by their similarly negative loadings in respect of PC1, ranging from -0.431 (SO42-) to -0.93 (TDS). Among the examined dissolved compounds SO42-and CH4 showed the least correlation with PC1 as indicated by loading values slightly below 0.5.

Preprints (www.preprints.org) | NOT PEER-REVIEWED | Posted: 14 December 2023 doi:10.20944/preprints202312.1097.v1

Relative to the PC2 axis the variables fall in two groups, characterized by negative and positive loadings respectively. The group of variables with negative PC2 loadings includes DIC, DOC, CO2, CH4, EEM PARAFAC components P1-P3, solid fraction . The PC2 loadings within this group vary from -0.66 (CH4) to -0.16 (EEM PARAFAC component P3). We denote this group of variables as "carbon-dominated", because it contains all the bulk carbon cycle parameters examined in this work. The group of positive PC2 loadings includes Na+, Cl-, SO42-, TDS, FI, EEM PARAFAC component P4, K+, DIN+, Ca2+, Mg2+. The PC2 loadings within this group are ranging from 0.14 (Na+) to 0.69 (Ca2+). We denote this group of variables as "salt-dominated", because it contains all the ionic compounds, except for HCO3- and CO32-, summarized as DIC. Within the "salt-dominated group" we observe a more or less pronounced relation in terms of PC2 loadings between K+, Na+ and Cl- as well as between Ca2+ and SO42-. Cl- as a major ion is closely related to TDS.

The humic-like DOM components P1, P2, P3 exhibit clear correlations among themselves, as well as to DOC, and S (%). In contrast, the protein-like component P4, representing freshly-derived autochthonous DOM, expresses no correlation neither to other EEM PARAFAC components, nor to any of the bulk dissolved carbon species. However, it weakly or moderately correlates to Mg2+, DIN and FI. Generally, the protein-like component P4 is associated with a "salt-dominated" group of variables on the PCA biplot as opposed to the humic-like components P1-P3 which are closely linked to the "carbon-dominated" group.

The analyzed ice samples are widely scattered across the biplot. The glacier ice samples from Severnaya Zemlya (SZ.G), included in the sample set as reference group for ground ice are remarkable for the highest positive loadings on PC1 at moderately negative values on PC2. The pure TGI samples from Marre-sale site in the Western Yamal (MS.TGI/p) appear to be quite similar to the glacier ice by the distribution of data points indicating the highest positive loadings on PC1 among the analyzed ground ice samples.

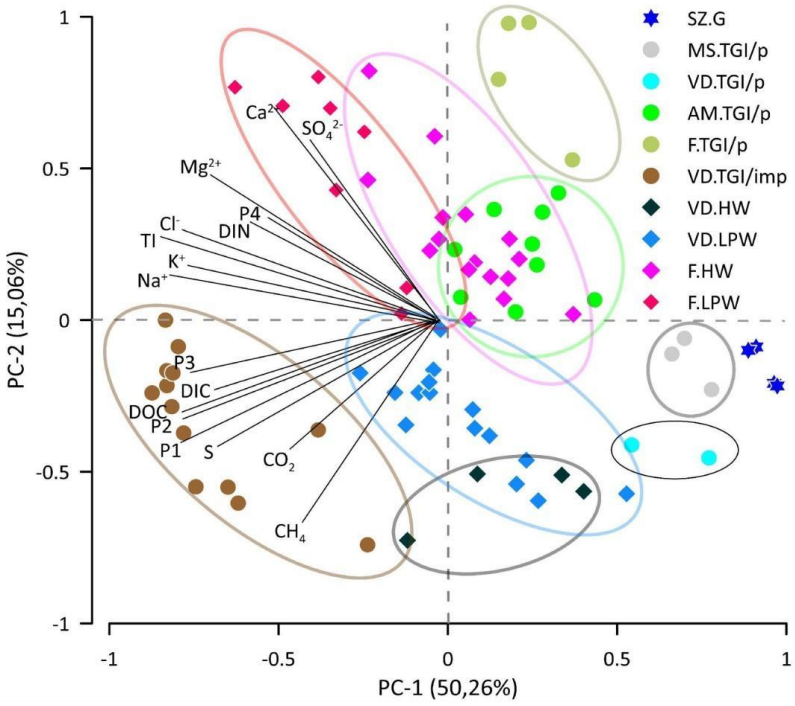

Figure 13. Biplot for the first two principal components, resulting the PCA analysis of the ground ice dataset. The ovals outline the data clouds of corresponding groups of the samples.

The pure TGI sampled near Amderma, Yugorsky peninsula (AM.TGI/p) are entirely located within the positive field of PC2 loadings indicating lower values on PC1 and higher on PC2 compared to the previous group of TGI (MS.TGI/p). Ice wedges sampled from the Fadeevsky Peninsula (F.TGI/p) have a range of the PC1 loadings similar to those of AM.TGI/p. samples, but considerably

 doi:10.20944/preprints202312.1097.v1

higher loadings on PC2 with maximum values in all the dataset. The last distinct group of TGI combines the samples from Vaskiny Dachi site, central Yamal (VD.TGI/imp), being referred to as impure ice, containing > 5% (42.01% on the average) of the solid fraction (S,%). Those samples are most divergent from the rest of the data points and characterized by the negative ranges of loadings on both PCs. VD.TGI/imp samples show minimum values on PC1 loadings in the dataset and vast scattering along the PC2 axis. PC1 and PC2 loadings for a sufficient part of the samples in this group are likely to be negatively correlated suggesting the simultaneous drop of PC1 and growth of PC2 loading values. The single samples VD.TGI/imp 6 and VD.TGI/imp 10 are most deviant from the other samples of this group, where the first one is notable for highest loading on PC1, but the second shows the highest value on PC2. Assuming the variables eigenvectors position on the biplot, the variation within the VD.TGI/imp sample set depends mainly on parameters of the "carbon-dominated" group of variables (DIC, DOC, CO2, CH4, EEM PARAFAC components P1-P3, solid fraction content).

The Late Pleistocene IWs sampled from retrogressive thaw slump of Vaskiny Dachi site, Central Yamal (VD.LPW), are distinguished by highly variable values of PC1 loadings (from medium positive to medium negative) and exclusively negative loadings of PC2. There is likely an inverse correlation between PC1 and PC2 loading values within this group as follows from the data clouds orientation on the biplot. Quite similar distribution pattern was observed for the samples VD.TGI/imp, but within the range of higher negative loadings on PC1. Four samples of Holocene IW (VD.HW) obtained in Vaskiny Dachi site are partly mixed on the biplot with Late Pleistocene IW (VD.LPW), but likely to be distinguished by slightly lower values of PC2 loadings. The sample VD.HW 3, remarkable for enormously high (for IW) solid fraction content (7.44%) and NH4+ concentration (5.15 mg/L), is highly divergent from other samples of the group and appears on the biplot closely to impure TGI sample VD.TGI/imp 10 with highest loading on PC1 in the VD.TGI/imp group. The IWs from the Fadeevsky Peninsula represent the last two groups of IWs in the dataset, both located on the biplot within the range of positive PC2 values, unlike the Yamal IW examined above. Holocene IWs (F.HW) are mostly falling into a positive range of PC1 axis, except for the samples F.HW 5 (803-5G), F.HW 9 and F.HW 10, indicating the negative loadings on PC1 coupled to elevated (positive) loadings on PC2. All of these samples are comparably enriched in major ions, especially in SO42-, while having an average level of DOC, DIC and fluorescent DOM components The most of the Late Pleistocene IWs samples from Faddeevsky (F.LPW) are characterized by the low (high negative) loadings on PC1 and high (positive) loadings on PC2, excluding the samples F.LPW 2 and F.LPW 6, notably depleted in solid fraction content (S,%), as well as in dissolved ions. The Holocene and Late Pleistocene IWs from Faddeevsky (F.HW. and F.LPW) are well separated by the PCs loadings distribution on the biplot.

5. Discussion

5.1. Variation of basic bulk parameters of the ground ice as indication of their biogeochemical heterogeneity

Our results show that the solid matter content (S,%) in the ground ice samples is likely a basic and reliable marker of variations between the chosen sample categories: pure tabular ground ice (TGI/p), impure tabular ground ice (TGI/imp) and ice wedges (IW, W). Apart from cryogenic mechanisms eventually driving the formation of relatively pure and relatively impure ground ice bodies, we propose that the solid fraction content is one of the critical parameters determining both bulk and individual chemical composition of ground ice samples, including the DOM fractions and the coupled DOC pool heterogeneity. The box-plots of the S (%) and TI (%) show coinciding patterns of the median values distribution (Figures 3, 4) which can preliminary indicate the solid material contacting source water as a major source of the dissolved salts. In the case of the ice wedges located near the sea coast, particularly the samples from Faddeevsky, marine aerosols may contribute to ion composition [12,29].

DOC concentrations in the analyzed ground ice samples are highly variable. The maximum for our dataset DOC content is encountered in the impure TGI (TGI/imp) with maximum and median

 doi:10.20944/preprints202312.1097.v1

values of 111.0 mg/L and 66.6 mg/L, respectively. Similar DOC loadings were reported for permafrost bogs, wetlands and coastal tundra [30]. Our values of DOC concentrations in the IW samples are generally in accordance with those previously reported for Western Siberia [18], Eastern Siberia and Alaska IWs [7]. We detected no significant variations in DOC content between the IWs from spatially remote geographical sections (Yamal and Yugorsky Peninsulas). Moreover, the Late Pleistocene and Holocene IWs from Faddeevsky exhibit a pair of median values (10.76 and 7.61 mg/L respectively) similar to the published for the Late Pleistocene and Holocene IW of East Siberia (11.1 and 7.3 mg/L respectively). The median DIC concentration is again extremely high (16.73 mg/L) in the organic rich impure TGI from Yamal (Vaskiny Dachi site). The intensive processes of microbial respiration could be responsible for the DIC enrichment in the host sediments and source water, if the carbonates leaching by water streams is rather unlikely. In other sampled locations the DIC values were comparable or lower than reported for ground ice of the Russian Arctic (the lowest is peculiar to pure TGI from Marre-Sale site).

The examined distribution of the bulk parameters is likely to indicate that the local environment with characteristic features of OM transportation and mineralization plays a crucial role in DOC and DIC enrichment or depletion. The major variation in terms of these parameters is associated with the ground ice types suggesting statistically distinct ranges of values. The minor intergroup variation may be also linked to the age of the IW.

5.2. Carbon-bearing gases (CH4 and CO2) concentrations characterizing the greenhouse gas storage and various conditions of the ground ice formation

Methane concentrations are extremely high in the impure TGI samples which is consistent with the published data on Western Siberia ground ice [18,31,32]. However, it is notable that the Yamal Late Pleistocene IWs are also extremely rich in methane. Although the median methane concentrations are 1.7 times higher in TGI (VD.TGI/imp), the IW (VD.LPW) are not statistically different from by CH4 values distribution. This generally suggests the source water enrichment in dissolved or/and gaseous methane before its incorporation into forming IW. Methane-rich host sediments are the most probable source of methane enrichment in Late Pleistocene IW from Vaskiny Dachi, explaining the observed resemblance between IW and TGI. At the same time IWs from Faddeevsky (both Late Pleistocene and Holocene) reveal more than 2000 times lower methane content, which may be due to both geographical factor, implying the lower biological activity in the higher latitudes, and the generally more favorable conditions for methanogenesis in the continental tundra biotopes (Vaskiny Dachi, Central Yamal) than in other settings (Faddeevsky, New Siberian islands).

The highest variability of methane content among all the measured and employed geochemical parameters is evident of the sporadic nature of methane distribution with contrasting zones of enrichment in the ground ice bodies with different genetic features. The cryogenic processes driving the segregation of gas saturation zones in permafrost may explain this phenomenon for TGI, characterized by epigenetic freezing [33]. We also cannot rule out the possibility of methane formation under cryogenic conditions that may also contribute to the observed methane variability [34]. The thawing methane rich ground ice deposits could be a considerable source of the predominantly ancient methane in the local ecosystems, however the rate of this contribution in the net methane emission is difficult to predict due to inhomogeneous methane distribution in the ground ice deposits.

Methane and carbon dioxide are partners in methane and carbon cycles suggesting that methane is readily oxidized by microorganisms either in aerobic or in anaerobic conditions (utilizing the wide-spread electron acceptors, such as SO42-, NO32- etc.) [35]. In our dataset, combining the TGI and IW there is no correlation between CH4 and CO2 which could have explained their relationships within a common carbon reservoir. In this regard our observations are consistent with the recent results published by [21], but in other works the negative correlation has been observed between CO2 and CH4 in the IWs [20,36]. Probably, there are many factors controlling the distribution and partitioning

 doi:10.20944/preprints202312.1097.v1

of the carbon-bearing gases, including the labile organic matter respiration and acetolactic methanogenesis, yielding CO2 coinciding with its uptake for hydrogenotrophic methanogenesis.

Summarizing the above we may conclude that for our dataset, Central Yamal TGI, categorized as impure (TGI/imp), containing > 10%, (~40% on an average) of solid fraction (S,%), together with Western Siberia IWs from Vaskiny Dachi site are the most important potential sources of the "direct emission" of methane upon thawing. All the other groups and types of the ground ice employed in this work seem to be negligible in this respect.

5.3. Fluorescent DOM composition and biolabile DOM fraction

In this work we examine the EEM PARAFAC components as the most reliable qualitative and quantitative indicators of the fluorescent DOM composition [22]. The fluorescent DOM is a significant part of the whole DOM, thus representing the features of the corresponding DOC partition. The valid PARAFAC model for a EEMs of a variety of the ground ice samples (n=216), including the various locations across Russian Arctic (Yamal Peninsula, Yugorsky Peninsula, Kotelny Island) approve the adequacy of the used approach. All the decomposed PARAFAC components were recognized through the EEM PARAFAC library search indicating the great resemblance with the components described in literature [26–28]. The composition of the fluorophores detected in the present work fully coincides with those published in our previous work [12] which was done on 119 EEM samples, including the similar range of the sample types. The finite PARAFAC dataset numbering 246 EEMs that was employed in the present work is fully containing the previous database. Regarding the linkage of our PARAFAC components to the fluorophores found in other ice and water samples from the cryosphere, we should notify the following. The humic-like DOM component P1, characterized by the longest excitation/emission (ex/em) wavelengths (370/470), is likely similar to KW5 (365/456) found in Yedoma IW of the Northeast Siberia [8] and to C2 (365/473) detected in glacial ice of southwest Greenland [37]. P1 was predominant in the Yamal impure TGI and less abundant in the TGI pure (Figure 10). P2 the shortest emission wavelength humic-like fluorophore (310/420) is likely to be relative to KW4 (300/420) of the Northeast Siberia IW [8] and C3 of the Greenland glacial ice [37], P3, the shortest excitation wavelength humic-like DOM (260/470), is resembled to KW1 [8] and Component 3 in the PARAFAC model comprising a great variety of glacier samples, from Canada to Antarctica [38]. The protein-like DOM component P4, classified as tryptophan-like, is rather close to the component 3, detected in the glacier DOM [38]. These observations exhibit a spectral composition integrity of fluorescent DOM in the cryosphere, suggesting either the certain commonality of the DOM sources within the sampled environments, or a convergence of various DOM species in their fluorescence features. We observe a satisfactory correlation between fluorescent DOM and DOC (Figure 11) approved by r2=0.96 (p=0.000), which is making it generally possible to use fluorescent DOM for a ground ice DOC structure semiquantative representation. Larger scattering of the data points in the field of relatively lower DOC values may indicate the presence of non-fluorescent DOM, which can be partly explained by the intercept in the linear regression equation (Figure 11).

The median composition of the ground ice fluorescent DOM indicates that the autochthonous protein-like component P4 is predominant in the glacier ice and pure TGI (TGI/p) samples, characterized by lower DOC concentrations. The highest loadings of both, DOC and fluorescent DOM are characteristic of the impure TGI (TGI/imp). P1, the longest wavelength fluorophore and probably the highest molecular weight humic-like DOM component among the identified fractions, is responsible for the observed DOC enrichment. The criterion of biolability is the most critical for a DOM composition assessment in the view of biogeochemistry. The low molecular weight and reduced aromaticity are considered major signatures of a labile DOM vulnerable to rapid biological oxidation/mineralization [39]. Assuming that, all the measured humic-like compounds (P1-P3) are rather recalcitrant compared to the nitrogen-rich protein-like component P4, ultimately linked to local microbial biomass. P4 is not correlated to the humic-like components indicating that autochthonous and allochthonous DOM fractions are likely to be disconnected in terms of a local biogeochemical cycling occurring in source water. Thus, the DOC-normalized values of P4 loadings can serve as a reliable tracer of a ground ice DOM biogeochemical "quality". However, as shown for

 doi:10.20944/preprints202312.1097.v1

East-Siberian Yedoma IWs the component KW4, coinciding with our humic like component P2 by the Ex/Em maximum was positively correlated with DOC loss (biodegradable DOC (BDOC) amount in standardized aerobic incubation experiments [8]). Thus, based on the literature data, we propose that component P2 may also be classified as biolabile and summed with component P4 to represent the speculative biolabile DOM fraction in our dataset. On the box plot (Figure 14) the distribution of this parameter is indicated for the particular groups of the ground ice samples. The statistically significant difference (Kruskall-Wallis multiple test) is observed between the biolabile DOM fraction of the pure TGI from Yugorsky peninsula (AM.TGI/p), impure TGI and Late Pleistocene IW from Central Yamal (VD.TGI/imp and VD.LPW, respectively), as well as between VD.TGI/imp and Holocene IW from New Siberian Islands (F.HW) as approved by $p<0.005$. Finally, we observe the following sequence of decreasing values of the speculative biolabile DOM fraction in the analyzed ground ice samples: AM.TGI/p > VD.TGI/p > F.HW > F.LPW > F.TGI/p > VD.LPW > VD.TGI/imp.

Summarizing the above, it can be argued that the ground ice samples from a great variety of settings contain a high molecular weight humic-like DOM as a major recalcitrant fraction of DOM (Components P1, P3) and low molecular weight humic like component (P2) plus autochthonous protein-like component (P4) as minor labile fraction of DOM. Therefore, the largest pool of DOC is associated with DOM, requiring an intensive enzymatic processing for generating substrates consumable by chemoorganotrophic microbiota, operating the aerobic and respiration coupled to CO2 and CH4 production in aerobic and anaerobic conditions respectively. The enzymatic processing, involving the cleavage of high-molecular weight compounds with increased aromaticity into low molecular weight aliphatic species is the most energy consuming stage of this catabolic pathway [8,11]. The excretion of the hydrolytic enzymes is coupled to significant carbon loss by the operating microbial biomass. The global role of the biolabile fraction is proposed not to be a direct quantitative conversion to greenhouse gases, but rather as providing a labile carbon source for production of the hydrolytic exoenzymes which are further responsible for involving the major pool of DOC in successive mineralization. This was approved by the published results of the experiments, implying the addition of IW thaw water, relatively enriched in ancient labile carbon, to modern permafrost soil leachates, relatively depleted in labile forms, that eventually leaded to the increased carbon loss in the experimental solutions [8]. Low solid fraction content in the ground ice deposits (except the impure TGI) may contribute upon their proposed thawing to the increase of water connectivity providing an effective transport within a disturbed zone of the low molecular weight DOM, highly vulnerable for microbial uptake and respiration. The combination of the current descriptive data on our ground ice geochemical composition with the further incubation tests, involving the published recommendation will allow to obtain a reliable data, which can be used for spatial generalization of the ground ice thawing influence on the modern Arctic ecosystems in terms of the carbon cycle.

Preprints (www.preprints.org) | NOT PEER-REVIEWED | Posted: 14 December 2023 doi:10.20944/preprints202312.1097.v1

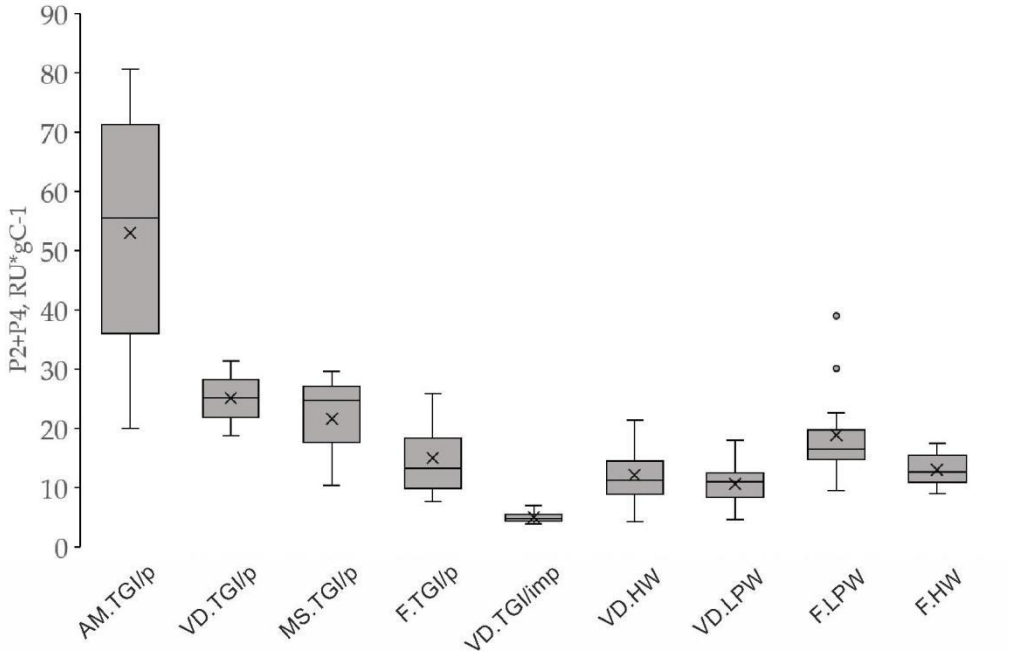

Figure 14. Boxplot of the biolabile fluorescent DOM (as sum of the components P2 and P4).

5.3. Variations in the ground ice samples geochemical composition and their possible drivers explained by exploratory statistical analysis

The results of PCA analysis (Figure 13) define the pronounced enrichment of the ice samples in dissolved compounds within a range between the glacial ice (employed as reference group) and impure TGI as the most pure and "contaminated" species of our dataset, respectively. The IWs of north-west Canada also showed the common driver for the solutes enrichment, expressed as high positive correlation of the measured ions with the first principal component [29]. Although, for those datasets ultimately comprising the IWs, marine aerosol transport was postulated as a predominant factor of solutes enrichment, in our case, including both IW and TGI, this is probably the contact with host sediments, however not excluding marine aerosols influence on the formation of nearshore Holocene IWs (Faddeevsky).

In spite of the definitely divergent genesis, the pure TGI samples from Marre Salle site (MS.TGI/p) appear to be convergently close to the glacier ice samples (SZ.G) in terms of the geochemical parameters distribution. Therefore, the corresponding ground ice bodies/layers are likely to contain virtually no solid inclusions and be very poor in the dissolved species analyzed (ions, DOC, gases etc.). The pure TGI samples from Vaskiny Dachi site (VD.TGI/p) are distinguished from those of Marre Salle (MS.TGI/p) by combination of low ion and DOC content with relatively elevated methane level (responsible for lower values of PC2). The pure TGI from Amderma site (AM.TGI/p) are mixed with Ice Wedges from Faddeevsky on PCA biplot, suggesting the geochemical convergence of the genetically different ice samples from spatially remote sites. However, there is a clear separation between Yamal and Faddeevsky IWs which is probably linked to variability in the ice formation conditions along the geographical scale or due to the other special horizontal variation in the ice formation environments. The outstanding abundance of methane featuring the Yamal IWs relative to the IWs of Faddeevsky clearly shows a better condition for methanogenesis and methane migration in corresponding environments, probably associated with more favorable conditions for basic biological productivity. The Holocene IW of the Yamal peninsula (VD.HW) shows a slightly different pattern of PCs distribution due to higher DOC and lower mineral content. The Holocene and Late Pleistocene IWs from Faddeevsky are also partly separated along the PC1 axis, with distinct groups of samples highly correlated to SO42- eigenvector due to the enrichment in none of sea-salt (nss) origin [12]. Impure TGI and Late Pleistocene IW from Yamal reveal the common patterns of distribution along the PC2 axis, which may be associated with the IW formation in the TGI body eventually responsible for their characteristic enrichment of methane and humic DOM.

 doi:10.20944/preprints202312.1097.v1

Humic-like DOM including the PARAFAC components P1-P3 obviously hosts the larger pool of DOC ultimately sourced by terrigenous higher plant debris. Gas compounds (CH4 and CO2) do not significantly correlate to any of the parameters, revealing a weak positive correlation to each other as well as to DOC and humic-like DOM. This can be explained by specific features of in- situ methane generation and transportation, which are totally different for IW and TGI. CO2, except for the equilibrium atmospheric constituent of the ice-captured air bubbles, is mainly associated with biological oxidation of OM and CH4 prior to freezing or under subsequent cryogenic conditions. Both DIC and CO2 correlate weakly or moderately with DOM components P1-P3, but do not correlate with the most biolabile P4 component (protein-like DOM). Thus, the autochthonous DOM is not predicting the intensity of OM mineralization in the ground ice source water, probably due to its minor contribution in C pools volumes. However, the refractory, but more abundant, humic-like components P1 and P2 are likely to be more quantitatively associated with both carbon pools: oxidized and reduced. Anyway, the interrelations between the individual parameters of the ground ice geochemical composition are very complicated and influenced by multiple factors related to the reaction and transportation processes operated within a wide timescale.

6. Conclusions

This study has revealed a high degree of variability in ground and glacier ice samples from various geographic locations when assessed through various geochemical parameters.

While material might be transported into the source water by various means, such as aerosol transport (particularly in the case of ice wedges), it appears that the interaction with solid material—such as sediments, detritus, and vegetation—is likely the overriding process in the ground ice enrichment in all the analyzed dissolved components.

Methane exhibits sporadic and contrasting distributions in the ground ice deposits, yet Yamal ground ice samples consistently show higher levels of methane compared to those from other geographical areas. Notably, methane concentrations are significantly high in both impure tabular ground ice (TGI), reaching up to 32281.65 ppmV, and Late Pleistocene ice wedges (IW), up to 14138.08 ppmV. This suggests that methane may be actively transported as bubbles or in solution from the surrounding sediments into the IW source water, subsequently becoming trapped during ice formation. The putative thawing of this methane-rich ground ice deposits should cause a detectable portion of methane as direct emission upon putative thawing.

The highest DOC concentration (up to 111 mg/L) was detected in the impure TGI from Yamal with extremely high gravimetric solid fraction content (>50%), the lower DOC content was encountered in the IW and the lowest in the pure TGI.

Excitation-Emission Matrix (EEM) Parallel Factor Analysis (PARAFAC) of Dissolved Organic Matter (DOM) allowed for the deconvolution of 4 components of fluorescent DOM (fDOM), which, as a sum, satisfactorily correlate to DOC. Terrigenous humic-like DOM, normally constituting the largest measured DOC pool, was predominant in all the analyzed ice samples except for glacier ice and pure TGI from Mare Sale (Western Yamal). The labile protein-like DOM, indicating an autochthonous source, showed no correlation to humic components and is proposed to be associated with microbial abundance in the ground ice [40]. The DOC of pure TGI samples exhibits the highest biogeochemical quality which may be responsible for the putative amplification of permafrost OM decomposition upon thawing [8,11].

The geochemical variables composition allows us to discern between Late Pleistocene and Holocene ice wedges from the Faddeevsky Peninsula, as well as to differentiate the Yamal ground ice from ground ice in other locations. However, there is a convergence in the geochemical composition between the tabular ground ice of Amderma and the Late Pleistocene ice wedges of the Faddeevsky Peninsula as well as between the glacial ice samples from Bolshevik Island. These results suggest the high potential of the applied methodology for both reconstructing paleoclimate conditions of the freezing environment and data classification for carbon cycle modeling.

Supplementary Materials: The following supporting information can be downloaded at the website of this paper posted on Preprints.org., Table S1: Mean concentrations and descriptive statistics of the ground ice groups; Table S2: All analytical data.

Author Contributions: Conceptualization, P.S. and A.P.; methodology, P.S., A.K., E.S., S.M., N.B. , A.L. and I.T.; software, W.H., P.S; writing—original draft preparation, P.S., A.P., A.K., E.S , N.B., P.G.; writing—review and editing; visualization, P.S., P.G., A.P.; supervision, I.S. and M.L. All authors have read and agreed to the published version of the manuscript.

Funding: This research was supported by the Russian Science Foundation, grant number 23-27-00123.

Data Availability Statement: Not applicable.

Acknowledgments: The authors would like to thank Victor Bogin (VNIIOkeangeologia) for the great assistance in the ground ice sample processing, anonymous reviewers for the detailed reports allowed to significantly improve the manuscript. Additionally, we thank the staff of the Earth Cryosphere Institute for their assistance in the field work.

Conflicts of Interest: The authors declare no conflict of interest. The funders had no role in the design of the study; in the collection, analyses, or interpretation of data; in the writing of the manuscript; or in the decision to publish the results.

References

1. Schuur, E.A.G.; McGuire, A.D.; Schädel, C.; Grosse, G.; Harden, J.W.; Hayes, D.J.; Hugelius, G.; Koven, C.D.; Kuhry, P.; Lawrence, D.M.; et al. Climate change and the permafrost carbon feedback. Nature 2015, 520, 171–179. https://doi.org/10.1038/na-ture14338.
2. Streletskaya I.D., Gusev E.A., Vasiliev A.A., Oblogov G.E., Molodkov A.N. Pleistocene—Holocene paleoenvironmental records from permafrost sequences at the Kara Sea coasts (NW Siberia, Russia) // Geography, Environment, Sustainability, 2013, v. 6, № 3, p. 60—76.
3. Vasiliev, A.A.; Melnikov, V.P.; Semenov, P.B.; Oblogov, G.E.; Streletskaya, I.D. Methane Concentration and Emission in Dominant Landscapes of Typical Tundra of Western Yamal. Dokl. Earth Sci. 2019, 485, 284–287.
4. Oblogov, G.E.; Vasiliev, A.A.; Streletskaya, I.D.; Zadorozhnaya, N.A.; Kuznetsova, A.O.; Kanevskiy, M.Z.; Semenov, P.B. Methane Content and Emission in the Permafrost Landscapes of Western Yamal, Russian Arctic. Geosciences 2020, 10, 412. https://doi.org/10.3390/geosciences10100412.
5. Yokohata, T., Saito, K., Ito, A. et al. Future projection of greenhouse gas emissions due to permafrost degradation using a simple numerical scheme with a global land surface model. Prog Earth Planet Sci, 2020, 7: 56. https://doi.org/10.1186/s40645-020-00366-8.
6. Zimov S A, Schuur E A G, Chapin F S. Permafrost and the global carbon budget. Science, 2006, 312: 1612–1613.
7. Fritz, M.; Opel, T.; Tanski, G.; Herzschuh, U.; Meyer, H.; Eulenburg, A.; Lantuit, H. Dissolved organic carbon (DOC) in Arctic ground ice. Cryosphere 2015, 9, 737–752.
8. Vonk J E, Mann P J, Davydov S, Davydova A, Spencer R G M, Schade J, Sobczak W V, Zimov N, Zimov S, Bulygina E, Eglinton T I, Holmes R M. High biolability of ancient permafrost carbon upon thaw.Geophys Res Lett, 2013, 40: 2689–2693.
9. Fellman J. B., Miller M. P., Cory R. M., D'Amore D. V., White D.; Characterizing Dissolved Organic Matter Using PARAFAC Modeling of Fluorescence Spectroscopy: A Comparison of Two Models; Environmental Science & Technology; 2009, 43(16): 6228-6234.
10. He, W.; Hur, J. Conservative behavior of fluorescence EEM-PARAFAC components in resin fractionation processes and its applicability for characterizing dissolved organic matter. Water Res. 2015, 83, 217–226. https://doi.org/10.1016/j.watres.2015.06.044.
11. Vonk J E, Tank S E, Mann P J, Spencer R G M, Treat C C, Striegl R G, Abbott B W, Wickland K P. Biodegradability of dissolved organic carbon in permafrost soils and aquatic systems: A meta-analysis. Biogeosciences, 2015, 12: 6915–6930.
12. Pismeniuk, A.; Semenov, P.; Veremeeva, A.; He, W.; Kozachek, A.; Malyshev, S.; Shatrova, E.; Lodochnikova, A.; Streletskaya, I. Geochemical Features of Ground Ice from the Faddeevsky Peninsula Eastern Coast (Kotelny Island, East Siberian Arctic) as a Key to Understand Paleoenvironmental Conditions of Its Formation. Land, 2023, 12, 324. https://doi.org/10.3390/land12020324.
13. Belova N.G., Babkina E.A., Dvornikov Y.A., Nesterova N.B., Khomutov A.V. Permafrost sediments with tabular ground ice on the coast of the Yugra Peninsula. Arctic and Antarctic, 2019, 4. DOI:10.7256/2453-8922.2019.4.3159.

14. Streletskaya, I.D.; Pismeniuk, A.A.; Vasiliev, A.A.; Gusev, E.A.; Oblogov, G.E.; Zadorozhnaya, N.A. The ice-rich permafrost sequences as a paleoenvironmental archive for the Kara Sea region (Western Arctic). Front. Earth Sci. 2021, 9, 723382. https://doi.org/10.3389/feart.2021.723382.
15. Govorukha L.S., Popova N.M.,Semenov I.V., Shamontieva L.A. Catalog of glaciers of the USSR. Volume 16. Angara-Yenisei region. Issue 1. Lenizdat, USSR, 1980.
16. Fritzsche, Diedrich & Schütt, Rainer & Meyer, Hanno & Miller, Heinz & Wilhelms, Frank & Opel, Thomas & Savatyugin, Lev. A 275 year ice-core record from Akademii Nauk ice cap, Severnaya Zemlya, Russian Arctic. Annals of Glaciology, 2005, 42: 361-366. 10.3189/172756405781812862.
17. Kotlyakov, V.M., S.M. Arkhipov, K.A. Henderson and O.V. Nagornov. Deep drilling of glaciers in Eurasian Arctic as a source of paleoclimatic records. Quat. Sci. Rev., 2004, 23(11–13), 1371–1390. doi:10.1016/j.quascirev.2003.12.0.
18. Semenov, P.B.; Pismeniuk, A.A.; Malyshev, S.A.; Leibman, M.O.; Streletskaya, I.D.; Shatrova, E.V.; Kizyakov, A.I.; Vanshtein, B.G. Methane and dissolved organic matter in the ground ice samples from Central Yamal: Implications to biogeochemical cycling and greenhouse gas emission. Geosciences 2020, 10, 450. https://doi.org/10.3390/geosciences10110450.
19. Yamamoto, S.; Alcauskas, J.B.; Crozier, T.E. Solubility of methane in distilled water and seawater. J. Chem. Eng. 1976, 21, 78–80.
20. Kim, K, Yang, J-W, Yoon, H, et al. Greenhouse gas formation in ice wedges at Cyuie, central Yakutia. Permafrost and Periglac Process. 2019; 30: 48–57. https://doi.org/10.1002/ppp.1994.
21. Yang, J-W, Ahn, J, Iwahana, G, et al. Origin of CO2, CH4, and N2O trapped in ice wedges in central Yakutia and their relationship. Permafrost and Periglac Process. 2023; 34(1): 122-141. doi:10.1002/ppp.2176.
22. Stedmon, C.A.; Bro, R. Characterizing dissolved organic matter fluorescence with parallel factor analysis: A tutorial. Limnol. Oceanogr.Methods 2008, 6, 572–579. https://doi.org/10.4319/lom.2008.6.57210.4319/lom.2008.6.572b.
23. Murphy, K. R. et al. Measurement of dissolved organic matter fluorescence in aquatic environments: an interlaboratory comparison. Environ. Sci. Technol. 2010, 44, 9405–9412, doi: 10.1021/es102362t.
24. Bro, R. PARAFAC. Tutorial and applications. Chemometr. Intell. Lab. Syst. 1997, 38, 149–171. https://doi.org/10.1016/S01697439(97)00032-4.
25. Parr, T.B.; Ohno, T.; Cronan, C.S.; Simon, K.S. comPARAFAC: A library and tools for rapid and quantitative comparison of dissolved organic matter components resolved by Parallel Factor Analysis. Limnol. Oceanogr.-Meth. 2014, 12, 114–125.
26. Fellman, J.B.; Hood, E. D'Amore; D.V.; Edwards, R.T.; White, D. Seasonal changes in the chemical quality and biodegradability of dissolved organic matter exported from soils to streams in coastal temperate rainforest watersheds. Biogeochemistry 2009, 95, 277–293.
27. Chen M. L., Price R. M., Yamashita Y., Jaffe R.; Comparative study of dissolved organic matter from groundwater and surface water in the Florida coastal Everglades using multi-dimensional spectrofluorometry combined with multivariate statistics; Applied Geochemistry, 2010, 25(6): 872-880.
28. Williams C. J., Yamashita Y., Wilson H. F., Jaffe R., Xenopoulos M. A.; Unraveling the role of land use and microbial activity in shaping dissolved organic matter characteristics in stream ecosystems; Limnology and Oceanography, 2010, 55(3): 1159-1171.
29. Holland KM, Porter TJ, Criscitiello AS,Froese DG. Ion geochemistry of a coastal ice wedge in northwestern Canada: Contributions from marine aerosols and implications for ice-wedge paleoclimate interpretations. Permafrost and Periglac Process. 2023;34(2):180-193. doi:10.1002/ppp.2184, https://onlinelibrary.wiley.com/doi/10.1002/ppp.2184.
30. Heffernan L, Dolly N. Kothawala1, Lars J. Tranvik. Review article: A systematic review of terrestrial dissolved organic carbon in northern permafrost. The Cryosphere, 2023 https://doi.org/10.5194/tc-2023-152 Preprint. Discussion started: 24 October.
31. Streletskaya, I.D.; Vasiliev, A.A.; Oblogov, G.E.; Streletskiy, D.A. Methane content in ground ice and sediments of the Kara Sea coast. Geosciences 2018, 8, 434. https://doi.org/10.3390/geosciences8120434.
32. Streletskaya, I.D.; Pismeniuk, A.A.; Vasiliev, A.A.; Gusev, E.A.; Oblogov, G.E.; Zadorozhnaya, N.A. The ice-rich permafrost sequences as a paleoenvironmental archive for the Kara Sea region (Western Arctic). Front. Earth Sci. 2021, 9, 723382. https://doi.org/10.3389/feart.2021.723382.
33. Kraev, G.; Schulze, E.-D.; Yurova, A.; Kholodov, A.; Chuvilin, E.; Rivkina, E. Cryogenic Displacement and Accumulation of Biogenic Methane in Frozen Soils. Atmosphere 2017, 8, 105.
34. Rivkina, E.; Shcherbakova, V.; Laurinavichius, K.; Petrovskaya, L.; Krivushin, K.; Kraev, G.; Pecheritsina, S.; Gilichinsky, D. Biogeochemistry of methane and methanogenic archaea in permafrost. FEMS Microbiol. Ecol. 2007, 61, 1–15.

35. Whiticar, M.J. Carbon and hydrogen isotope systematics of bacterial formation and oxidation of methane. Chem. Geol., 1999, 161: 291–314.
36. Brouchkov, A.; Fukuda, M. Preliminary measurements on methane content in permafrost, Central Yakutia, and some experimental data. Permafr. Periglac. Process. 2002, 13, 187–197. https://doi.org/10.1002/ppp.422.
37. Kellerman, A.M.; Hawkings, J.R.; Wadham, J.L.; Kohler, T.J.; Stibal, M.; Grater, E.; Marshall, M.; Hatton, J.E.; Beaton, A.; Spencer, R.G.M. Glacier outflow dissolved organic matter as a window into seasonally changing carbon sources: Leverett Glacier, Greenland. JGR Biogeosci. 2020, 125, e2019JG005161. https://doi.org/10.1029/2019JG005161.
38. Dubnick A, Barker J, Sharp M, et al. Characterization of dissolved organic matter (DOM) from glacial environments using total fluorescence spectroscopy and parallel factor analysis. Annals of Glaciology, 2010, 51(56):111-122. doi:10.3189/172756411795931912.
39. Hudson, N.; Baker, A.; Reynolds, D. Fluorescence analysis of dissolved organic matter in natural, waste and polluted waters-a review. Riv. Res. Applic. 2007, 23, 631–649.
40. Bixi Guo, Wei Li, Pamela Santibáñez, John C. Priscu, Yongqin Liu, Keshao Liu. Organic matter distribution in the icy environments of Taylor Valley, Antarctica. Science of The Total Environment, 2022, 841: 1. https://doi.org/10.1016/j.scitotenv.2022.156639.